JOURNAL OF AIRCRAFT
Vol. 29, No. 3, May–June 1992

Extension and Validation of an Unsteady Wake Model for Rotors

Ay Su,* Kyung M. Yoo,† and David A. Peters‡
Georgia Institute of Technology, Atlanta, Georgia 30332

A new three-dimensional, finite-state induced-flow model is extended to treat nonlinearities associated with the mass flow induced through the rotor plane. This new theory is then applied to the correlation of a recent set of unsteady, hover laser Doppler velocimetry inflow measurements conducted in the Aeroelastic Rotor Test Chamber at Georgia Institute of Technology. Although the model is intended primarily as a representation of unsteady aerodynamics for aeroelasticity applications, the results show that it has an excellent capability in predicting the inflow distribution in hover except near the root and tip. In addition, the computed unsteady spanwise lift distribtuion of a rotor is compared with that from an unsteady vortex lattice method for pitch oscillations at various frequencies. The new model is shown to be capable of prediction of unsteady loads typical of aeroelastic response.

Nomenclature

$[A^m]$, $[B^m]$ = matrices of integrals
a = slope of lift curve, 1/rad
a_n^m, b_n^m = induced flow coefficients (in the rotating system)
B_{nj}^{mr} = integrals
C_n^m, D_n^m = coefficients of potential functions
C_T = thrust coefficient
c = blade chord, ft
$\bar{c}$ = dimensionless blade chord, c/R
E_n^m, F_n^m = inflow integrals
G_n^m = apparent mass diagonals
g_n^m = complex inflow variables
H_n^m = combination of factorials
J = number of blade-passage harmonics
j = polynomial number
L_q = lift per unit span of qth blade divided by $\rho\Omega^2R^3$
M = number of harmonics
m = harmonic number index
$(m)!!$ = $(m)(m-2)(m-4)\cdots(2 \text{ or } 1)$
n = polynomial number
$P_n^m(\nu)$ = Legendre functions
$\bar{P}_n^m(\nu)$ = normalized functions, $(-1)^m P_n^m(\nu)/\rho_n^m$
Q = number of blades
$Q_n^m(i\eta)$ = associated Legendre functions
q = blade index
R = rotor radius, ft
$\bar{r}$ = radial position normalized on R
r = harmonic number index
S = number of shape functions per harmonic
t = time, s
$\bar{t}$ = nondimensional time, Ωt
V = mass-flow parameter, $V_\infty + 2\bar{\nu}$
V_n = elements of diagonal mass-flow matrix
V_T = total velocity across the disk, $V_\infty + \bar{\nu}$
v = induced velocity at rotor disc divided by ΩR
z = coordinate normal to rotor divided by R, positive above rotor
α_n^m, β_n^m = induced flow coefficients (in the nonrotating system)
δ_{ij} = Kronecker delta, 1 if $i = j$, otherwise 0
η = ellipsoidal coordinate, 0 on disc
θ = unsteady pitch angle
θ_q = pitch angle of qth blade, $\theta_0 + \tilde{\theta}\cos\omega(\bar{t} + \phi_q)$
θ_0 = steady pitch angle
ν = ellipsoidal coordinate, $\sqrt{1-\bar{r}^2}$ on disk
$\bar{\nu}$ = momentum-theory value of induced flow, $C_T = 2\bar{\nu}|V_\infty + \bar{\nu}|$
$\tilde{\nu}$ = perturbation induced velocity
ρ_n^m = normalization factor, $\sqrt{\frac{1}{2n+1}\frac{(n+m)!}{(n-m)!}}$
σ = rotor solidity, $\bar{c}Q/\pi$
τ_n^{mc}, τ_n^{ms} = coefficients of pressure expansion
$\Phi(\nu, \eta, \bar{\psi}, \bar{t})$ = potential function, nondimensional pressure
$\phi(\bar{r}, \psi, \bar{t})$ = pressure across the disk divided by $\rho\Omega^2R^2$
$\phi_n^m(\bar{r})$ = inflow shape functions, $\bar{P}_n^m(\nu)/\nu$
ϕ_q = phase shift of qth blade
ψ = azimuthal position on rotor disc, rad
$\bar{\psi}$ = ellipsoidal coordinate, ψ on disc
ψ_q = spatial position of qth blade, rad
$\bar{\psi}_q$ = relative position of qth blade, $(q-1)2\pi/Q$
Ω = rotor speed, rad/s
ω = nonrotating frequency, /rev
$\{\}$ = column matrix
$< >$ = row matrix

Superscripts

$\tilde{}$ = perturbation components
$\bar{}$ = steady components, except $\bar{t}$
$\hat{}$ = rotating system
$*$ = $\partial/\partial\bar{t}$

Received Sept. 1, 1990; revision received Jan. 15, 1991; accepted for publication April 6, 1991.

*Postdoctoral Fellow, School of Aerospace Engineering.
†Graduate Research Assistant, School of Aerospace Engineering.
‡Professor, School of Aerospace Engineering. Associate Fellow AIAA.

Introduction

PROPER modeling of unsteady aerodynamic effects is an important ingredient in aeroelastic stability and response calculations for rotary-wing applications. The basic physical components of a helicopter blade and their relationships to each other are shown graphically in Fig. 1. The rotor is divided into three basic theoretical models: blade aerodynamics, blade

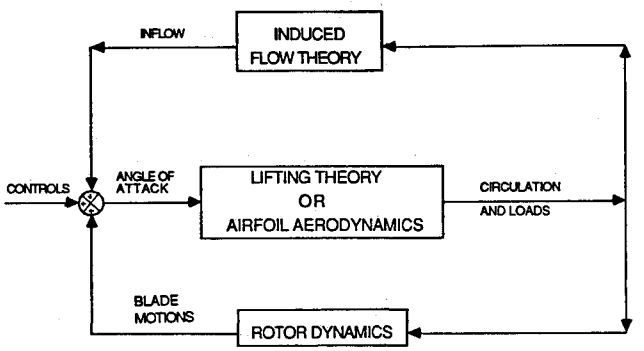

Fig. 1 Block diagram of inflow dynamics.

structural dynamics, and external flowfield. In the forward loop, the flowfield at the blade (e.g., angle of attack, flow gradients, rates, etc.) feeds into the blade airfoil theory (which can range in complexity from blade-element theory, through lifting-surface and dynamic-stall theories, all the way to complex Navier-Stokes solvers) to give the lift and circulation developed on the blade. The upper feedback loop relates the time history of circulatory lift on the blade to the resultant induced flow at the blade, which is calculated, for example, by the Biot-Savart Law, dynamic inflow models, or vortex wake models. The induced flow is fed back into the angle of attack to create unsteady aerodynamics. In the lower feedback loop, blade lift is provided to a blade structural dynamic model to provide blade motions that, in turn, change the blade angle of attack and thereby impact aeroelastic stability.

It is important to note that the blade lifting theory, the induced flow theory, and the blade dynamic model can be formulated independently of each other. However, the highly coupled nature of these three theories suggests that, for a model to be useful for rotor aeroelasticity, it must be capable not only of filling the appropriate blocks with reasonable algorithms, but it must also have appropriate coupling capability so that the loops can be closed with computational efficiency. Strictly speaking, modeling for aeroelasticity (as contrasted with performance) further requires that the individual models have explicitly defined state variables. If structural and aerodynamic states are not defined, then conventional Floquet and eigenvalue stability analysis cannot be performed.

Previous Work

Detailed descriptions of past research in unsteady aerodynamic theories for rotors can be found in Refs. 1–6. Rotor theories may generally be categorized into classical two-dimensional unsteady aerodynamic theories,[1,2] vortex-filament theories,[3,4] and finite-state models.[5,6] Of the two-dimensional theories, Theodorsen theory is inadequate for rotor analysis because of its inappropriate wake assumption.[7] Loewy theory also is deficient in that 1) it is two dimensional and only applies to linear aerodynamics of a flat-plate airfoil, and 2) it is in the frequency domain and thus inappropriate for conventional aeroelastic eigenvalue analysis (with the possible exception of *V-g* plots for the stability boundary in hover).

Recent developments in vortex-filament analysis use more complex, discretized wake geometries. For example, there are prescribed-wake lifting-line theories,[8] free-wake lifting-line theories,[9] and lifting-surface theories.[10] The induced-flow calculation (i.e., the upper feedback loop) of these vortex theories is found from the Biot-Savart Law as applied to the geometry of the wake. Therefore, they can overcome all of the deficiencies of Loewy theory and provide adequate prediction of rotor performance.

However, if one is interested in blade dynamics and aeroelasticity, these theories do not easily lend themselves to linearization and eigenvalue analysis. First of all, these models are computationally intensive in tracking the unsteady vorticity and in computing induced-flow integrals over hundreds of filaments at every time step. Second, they contain hidden state variables that cannot be accounted for within conventional linear-system formulations. Therefore, these models, although important tools for helicopter performance analysis, are not presently viable alternatives for aeroelastic analysis of a realistic rotor.

Based on this need for an advanced wake model that allows direct computation of Floquet or constant-coefficient eigenvalues (while not precluding time-history or frequency-domain analyses), a new, three-dimensionl, finite-state, generalized wake model has been developed.[7] This model is based on actuator-disk theory, but modified so as to be unsteady and to have a finite number of blades. It takes as input whatever circulatory lift distribution is present (regardless of the source). The states of the model are the coefficients of combined azimuthal harmonics and radial shape functions that describe the induced flowfield. More important, these states obey ordinary differential equations that may be written in the time or frequency domain. Therefore, this model is well suited for aeroelastic analysis.

Preliminary results in Ref. 7 show that this model captures Loewy theory, contains the near-wake approximation for the Theodorsen function, and includes dynamic inflow theory implicitly. In forward flight applications,[11] the correlation with measurement inflow data at the U.S. Army's Langley facility is as good, or better than, that of three-dimensional vortex theories. The results of elastic-blade eigenvalue analysis in hover can be found in Ref. 12. At frequencies near integer multiples of the rotor speed, the induced flow is dominated by shed vorticity, but away from these resonances, it is dominated by trailing vorticity.

Scope of Work

In this paper, we provide further extension and validation of this new model in hover and axial flight. First, the theory is extended to include the importance of nonlinearities in hover. Also, a computational method is developed to calculate the frequency response of the induced flow in an efficient manner. This formulation is important because it allows superposition of the unsteady inflow with the steady inflow to obtain the total inflow. Analytic predictions of induced flow due to both steady and unsteady pitch angles are compared with experimental data obtained in the Aeroelastic Rotor Test Chamber at Georgia Institute of Technology (hereafter refered to as AEROTECH). Also, the spanwise lift distribution for a two-bladed rotor, for both collective and differential modes, is compared with results of an unsteady vortex lattice method[3] and with two-dimensional quasisteady aerodynamics.

Description of Wake Model

The detailed theoretical background of this unsteady wake model is described in Ref. 5. The centerpiece of the theory is based on Prandtl's acceleration potential function,[13] which satisfies Laplace's equation and also gives a pressure discontinuity across a circular disc:

$$\Phi(\nu, \eta, \bar{\psi}, \bar{t}) = \sum_{m,n} P_n^m(\nu) Q_n^m(i\eta)[C_n^m(\bar{t})\cos(m\bar{\psi}) + D_n^m(\bar{t})\sin(m\bar{\psi})] \quad (1)$$

It follows that the pressure across the rotor disc is the difference between the upper and lower pressure. Thus, we have

$$\phi(\bar{r}, \psi, \bar{t}) = \sum_{n,m} \bar{P}_n^m(\nu)[\tau_n^{mc}(\bar{t})\cos(m\psi) + \tau_n^{ms}(\bar{t})\sin(m\psi)] \quad (2)$$

where

$$\bar{P}_n^m(\nu) = (-1)^m P_n^m/\rho_n^m$$
$$\tau_n^{mc} = (-1)^{m+1}2Q_n^m(i0)C_n^m\rho_n^m$$
$$\tau_n^{ms} = (-1)^{m+1}2Q_n^m(i0)D_n^m\rho_n^m$$
$$\rho_n^m = \sqrt{\frac{1}{2n+1}\frac{(n+m)!}{(n-m)!}}$$

We may expand the induced velocity at the disk in terms of harmonics and arbitrary radial functions (in a similar manner to the expansion of the acceleration potential function). This gives

$$v(\bar{r}, \psi, \bar{t}) = \sum_{n,m} \phi_n^m(\bar{r})[\alpha_n^m(\bar{t})\cos(m\psi) + \beta_n^m(\bar{t})\sin(m\psi)] \quad (3)$$

where the coefficients $\alpha_n^m(\bar{t})$ and $\beta_n^m(\bar{t})$ are the states of the model, and $\phi_n^m(\bar{r})$ are the radial expansion functions $\bar{P}_n^m(\nu)/\nu$, where $\bar{r} = \sqrt{1-\nu^2}$. As it turns out, $\phi_n^m(\bar{r})$ are simply polynomials in $\bar{r}$. In Eqs. (1–3), m assumes all values from 0 to M, and n takes on only the values $m+1$, $m+3$, $m+5$, etc. Note, m and r are dummy indices that take on the values, 0, . . . M to create matrix partitions.

In axial flow, the governing differential equations become

$$\begin{pmatrix} \ddots & & \\ & G_n^m & \\ & & \ddots \end{pmatrix}\begin{Bmatrix} \vdots \\ \{\alpha_j^m\} \\ \vdots \end{Bmatrix}^* + 2V_\infty \begin{pmatrix} \ddots & & \\ & [B_{nj}^r] & \\ & & \ddots \end{pmatrix}\begin{Bmatrix} \vdots \\ \{\alpha_j^r\} \\ \vdots \end{Bmatrix} = \begin{Bmatrix} \vdots \\ \{\tau_n^{mc}\} \\ \vdots \end{Bmatrix} \quad (4)$$

where ( )* implies a nondimensional time derivative, V_∞ is the freestream velocity, and

$$B_{nj}^m \equiv \int_0^1 \bar{P}_n^m\bar{P}_j^m/\nu \, d\nu = \int_0^1 \phi_n^m\phi_j^m\bar{r} \, d\bar{r}$$
$$= \sqrt{\frac{H_j^m}{H_n^m}}(-1)^{\frac{n+j-2m-2}{2}}\sqrt{(2n+1)(2j+1)}$$
$$\times \sum_{q=m,m+2}^{j-1} H_q^m \frac{2q+1}{(n-q)(n+q+1)} \quad (5)$$

$$G_n^m = \frac{4}{\pi}H_n^m \quad (6)$$

$$H_n^m = \frac{(n+m-1)!!(n-m-1)!!}{(n+m)!!(n-m)!!} \quad (7)$$

$$\tau_n^{0c} = \frac{1}{2\pi}\sum_{q=1}^{Q}\int_0^1 L_q(\bar{r}, \bar{t})\phi_n^0 \, d\bar{r} \quad (8)$$

$$\tau_n^{mc} = \frac{1}{\pi}\sum_{q=1}^{Q}\int_0^1 L_q(\bar{r}, \bar{t})\phi_n^m \, d\bar{r}\cos(m\psi_q) \quad (9)$$

A similar set of equations exists for β_n^m except that $m = 0$ is not present, and $\cos(m\psi_q)$ must become $\sin(m\psi_q)$ in the τ terms.

Thus, this unsteady model is essentially a linear relation between the perturbation inflow components and the forces acting on the rotor disk. These inflow components become the degrees of freedom of the dynamic system. Furthermore, this model is able to include higher frequency unsteady aerodynamics as more inflow harmonics are added.

Linearized Extension

In order to derive a more general version, we begin with the assumption that

$$\text{total velocity across disk} = V_\infty + \bar{\nu} + \tilde{\nu} \quad (10)$$

where V_∞ is the freestream across the rotor disk, $\bar{\nu}$ the steady induced velocity, and $\tilde{\nu}$ the unsteady perturbation induced velocity.

Therefore, one component of the momentum equation in vertical flight is

$$\frac{\partial\tilde{\nu}}{\partial\bar{t}} + (V_\infty + \bar{\nu} + \tilde{\nu})\left(\frac{\partial\bar{\nu}}{\partial z} + \frac{\partial\tilde{\nu}}{\partial z}\right) = -\left(\frac{\partial\bar{\Phi}}{\partial z} + \frac{\partial\tilde{\Phi}}{\partial z}\right) \quad (11)$$

where $\bar{\Phi}$ is simply pressure (not necessarily an acceleration potential) and z is the direction normal to the disk. Equation (11) can be divided into the steady part

$$(V_\infty + \bar{\nu})\frac{\partial\bar{\nu}}{\partial z} = -\frac{\partial\bar{\Phi}}{\partial z} \quad (12)$$

and the perturbation part

$$\frac{\partial\tilde{\nu}}{\partial\bar{t}} + (V_\infty + \bar{\nu})\frac{\partial\tilde{\nu}}{\partial z} + \tilde{\nu}\frac{\partial\bar{\nu}}{\partial z} = -\frac{\partial\tilde{\Phi}}{\partial z} \quad (13)$$

where perturbations squared are neglected.

If we further assume that the ratio of the downstream variations of $\bar{\nu}$ and $\tilde{\nu}$ (with respect to their values at the disk) are proportional to each other, which is reasonable since $\bar{\nu}$ and $\tilde{\nu}$ appear together in Eq. (10), then we may write

$$\frac{(\partial\bar{\nu}/\partial z)}{\bar{\nu}} = \frac{(\partial\tilde{\nu}/\partial z)}{\tilde{\nu}} \quad (14)$$

It follows that Eq. (13) can be written as

$$\frac{\partial\tilde{\nu}}{\partial\bar{t}} + (V_\infty + 2\bar{\nu})\frac{\partial\tilde{\nu}}{\partial z} = -\frac{\partial\tilde{\Phi}}{\partial z} \quad (15)$$

Thus, a different mass-flow parameter, $V_\infty + 2\bar{\nu}$, appears on the coefficient of the momentum flux term. Therefore, in Eq. (4), which comes directly from the momentum equation,[5] we can replace V_∞ by the more general V, defined as

$$V = V_\infty + 2\bar{\nu} \quad (16)$$

A detailed discussion of using this mass-flow parameter in the calculation of the equivalent Lock number and the advantage over other flow parameters can be found in Ref. 14. This modification extends our linearized, acceleration-potential method to a greater range of validity, including hover ($V_\infty = 0$).

Nonlinear Extension

According to Ref. 15, the steady and perturbation thrust (as well as the steady and perturbed induced flow) for dynamic inflow can be combined to obtain a nonlinear induced-flow model that is not entirely a perturbation theory. Here, we make a similar extension to our complete induced-flow formulation. First, recall that V_∞ of Eq. (4) has been replaced by the mass-flow parameter V, which can be expressed as a diagonal matrix of V in Eq. (4). For the nonlinear version, we follow Ref. 15 and replace the first diagonal element of this matrix by $V_T = V_\infty + \bar{\nu}$, which is the total resultant flow through the disk. All other elements remain as V. The new diagonal matrix is expressed as $[V]$ for convenience.

There can be two versions of this nonlinear inflow model. If we take $[V]$ to the right of the B matrix, the nonlinear inflow model thus becomes

$$\begin{pmatrix} \ddots & & \\ & G_n^m & \\ & & \ddots \end{pmatrix}\begin{Bmatrix} \vdots \\ \{\alpha_j^m\} \\ \vdots \end{Bmatrix}^* + \begin{pmatrix} \ddots & & \\ & [B_{nj}^r] & \\ & & \ddots \end{pmatrix}$$
$$\times \begin{pmatrix} \ddots & & \\ & 2V_n & \\ & & \ddots \end{pmatrix}\begin{Bmatrix} \vdots \\ \{\alpha_j^r\} \\ \vdots \end{Bmatrix} = \begin{Bmatrix} \vdots \\ \{\tau_n^{mc}\} \\ \vdots \end{Bmatrix} \quad (17)$$

where α_j^m and τ_n^{mc} now imply the total inflow and loads. In order for Eq. (17) to linearize to Eq. (4), $[V]$ must depend on the inflow in the following way:

$$V_1 = V_T = |V_\infty + \bar{v}|, \quad V_n = V = |V_\infty + 2\bar{v}| n \neq 1$$

$$\bar{v} = \sqrt{3}\alpha_1^0 = \frac{2}{\sqrt{3}} B_{11}^0 \alpha_1^0$$

This implies for the steady state that

$$\{\tau_j^{0c}\} = 2V_1\alpha_1^0\{B_{1j}^0\}$$

$$C_T = 2V_1\bar{v}$$

Thus, the theory is nonlinear in the uniform component of inflow α_1^0. The other version of the nonlinear inflow model in obtained if we take $[V]$ to the left of the B matrix. Then, the inflow model becomes

$$\begin{pmatrix} \ddots & & \\ & G_n^m & \\ & & \ddots \end{pmatrix} \begin{Bmatrix} \vdots \\ \{\alpha_j^m\} \\ \vdots \end{Bmatrix}^* + \begin{pmatrix} \ddots & & \\ & 2V_n & \\ & & \ddots \end{pmatrix} \begin{pmatrix} \ddots & & \\ & [B_{nj}^r] & \\ & & \ddots \end{pmatrix} \begin{Bmatrix} \vdots \\ \{\alpha_j^r\} \\ \vdots \end{Bmatrix} = \begin{Bmatrix} \vdots \\ \{\tau_n^{mc}\} \\ \vdots \end{Bmatrix} \tag{18}$$

In order for Eq. (18) to linearize to Eq. (4), $[V]$ must depend on the inflow in a different way from Eq. (17):

$$V_1 = V_T, \quad V_n = V \quad \text{if} \quad n \neq 1 \quad \bar{v} = \frac{2}{\sqrt{3}} < B_{1j}^0 > \{\alpha_{1j}^0\}$$

This implies that, for the steady state,

$$\{\alpha_j^0\} = \frac{\sqrt{3}}{4}\frac{C_T}{V_1}\{A_{j1}^0\}$$

where $\{A\}$ has a closed-form representation[6] and corresponds to an elliptical inflow (and lift) distribution. Thus, this second version is nonlinear in the elliptical component of inflow.

Both Eqs. (17) and (18) reduce to classical, nonlinear momentum theory when only one inflow distribution (uniform or elliptical) is assumed. Also, when perturbed about that steady inflow, both give a perturbation inflow according to Eq. (4), with V_∞ replaced by V. Thus, either could be considered a viable candidate for a nonlinear inflow model. (The theories are nonlinear in the sense that V_n depends on α_j^0, thus giving quadratic terms in α_j^0.) As we will see later, however, the true flow for most rotors is closer to uniform than to elliptical, which makes Eq. (17) a better choice.

Rotating System

In axial flow, it is advantageous to rewrite the inflow model in the rotating system. To do this, a reference blade needs to be chosen first; and, thus, the azimuthal position of any blade ψ_q can be represented with respect to the reference blade

$$\psi_q = \bar{t} + \hat{\psi}_q \tag{19}$$

where $\bar{t}$ is the position of the reference blade in the nonrotating system and

$$\hat{\psi}_q = \frac{2\pi}{Q}(q - 1) \tag{20}$$

Hence, Eq. (3) can be rewritten as

$$v(\bar{r}, \psi, \bar{t}) = \sum_{n,m} \phi_n^m(\bar{r})[a_n^m\cos(m\hat{\psi}) + b_n^m\sin(m\hat{\psi})] \tag{21}$$

where

$$\begin{Bmatrix} a_n^m \\ b_n^m \end{Bmatrix} = \begin{bmatrix} \cos(m\bar{t}) & \sin(m\bar{t}) \\ -\sin(m\bar{t}) & \cos(m\bar{t}) \end{bmatrix} \begin{Bmatrix} \alpha_n^m \\ \beta_n^m \end{Bmatrix} \tag{22}$$

The new governing differential equations for perturbation inflow thus become

$$\begin{bmatrix} \ddots & & \\ & [G_n^m] & \\ & & \ddots \end{bmatrix} \begin{Bmatrix} \vdots \\ \{a_j^m\} \\ \vdots \\ \{b_j^m\} \\ \vdots \end{Bmatrix}^* + \begin{bmatrix} \ddots & & \ddots & \\ & 2[B_{nj}^m][V] & & -m[G_n^m] \\ \ddots & & \ddots & \\ & m[G_n^m] & & 2[B_{nj}^m][V] \\ & & \ddots & \end{bmatrix} \times \begin{Bmatrix} \vdots \\ \{a_j^m\} \\ \vdots \\ \{b_j^m\} \\ \vdots \end{Bmatrix} = \begin{Bmatrix} \vdots \\ \{\hat{\tau}_n^{mc}\} \\ \vdots \\ \{\hat{\tau}_n^{ms}\} \\ \vdots \end{Bmatrix} \tag{23}$$

where a_n^m and b_n^m now couple, and

$$\hat{\tau}_n^{0c} = \tau_n^{0c} = \frac{1}{2\pi}\sum_q \int_0^1 L_q\phi_n^0(\nu)\, d\bar{r} \tag{24}$$

$$\hat{\tau}_n^{mc} = \tau_n^{mc}\cos(m\bar{t}) + \tau_n^{ms}\sin(m\bar{t}) = \frac{1}{\pi}\sum_q \int_0^1 L_q\phi_n^m(\nu)\, d\bar{r}\cos(m\hat{\psi}_q) \tag{25}$$

$$\hat{\tau}_n^{ms} = -\tau_n^{mc}\sin(m\bar{t}) + \tau_n^{ms}\cos(m\bar{t}) = \frac{1}{\pi}\sum_q \int_0^1 L_q\phi_n^m(\nu)\, d\bar{r}\sin(m\hat{\psi}_q) \tag{26}$$

Thus, Eqs. (23–26) give the nonlinear dynamic wake equations in the rotating system.

Lift Model

For the present method of unsteady aerodynamics, the lift must be expressible as an explicit function of the velocity field at the blade. Thus, lift theories that implicitly include induced flow (e.g., through a lift deficiency function) are not applicable for L_q. One acceptable theory is quasisteady, two-dimensional aerodynamics but with induced flow appearing explicitly in the angle of attack. (That is what is used here.) This gives the circulatory lift on the qth blade

$$L_q(\bar{r},\bar{t},\psi_q) = \frac{\bar{c}a}{2}[\theta_q(\bar{t})\bar{r}^2 - \bar{r}v(\psi_q) + \frac{1}{2}\bar{r}\bar{c}\theta_q^*] \tag{27}$$

where $v(\psi_q)$ is the induced flow at the qth blade.

At first glance, one might object to the use of two-dimensional, quasisteady lift in a three-dimensional unsteady analysis. Recall, however, that the inclusion of induced flow in Eq. (27) closes the unsteady feedback loop. Thus, Eq. (27) actually represents full unsteady aerodynamics. It is quasisteady only in the sense that the flow boundary conditions at the airfoil are quasisteady. Also, one should not include apparent-mass lift in Eq. (27). Apparent-mass terms contribute to lift but not to shed vorticity.

Frequency Domain

Although we see the primary utilization of our model to be in the time domain, the validations in this paper are done in the frequency domain to facilitate comparisons with other theories and tests. A generalized formula can be derived to compute the induced flow under static plus oscillatory pitch angle (i.e., $\theta = \theta_0 + \tilde{\theta}\cos\omega\bar{t}$). This derivation is done in the frequency domain and in the rotating system and is related to a lift deficiency function. To begin, we define a complex inflow variable in the rotating system g_n^m

$$g_n^0 = a_n^0 \tag{28}$$

$$g_n^m = \frac{a_n^m - ib_n^m}{2} \tag{29}$$

$$g_n^{-m} = \frac{a_n^m + ib_n^m}{2} \tag{30}$$

Then, we assume simple harmonic motion for g_n^m

$$g_n^m = \tilde{g}_n^m e^{i\omega\bar{t}}, \qquad a_n^m = \tilde{a}_n^m e^{i\omega\bar{t}}, \qquad b_n^m = \tilde{b}_n^m e^{i\omega\bar{t}} \tag{31}$$

Based on the blade-element model of Eq. (27), the oscillatory lift can be expressed as

$$\text{lift} = \frac{\bar{c}a}{2}\bar{r}^2\left(\tilde{\theta} - \frac{v}{\bar{r}} + \frac{1}{2}\bar{c}\tilde{\theta}i\omega/\bar{r}\right) \tag{32}$$

By substituting Eqs. (28–32) into Eq. (23), we obtain for a single-bladed rotor

$$\tilde{g}_j^r = \left[-i(m-\omega)G_n^m\delta_{mr} + \left(2V\delta_{mr} + \frac{\sigma a}{4}\right)B_{nj}^{mr}\right]^{-1} \times \left(\frac{\sigma a}{4}\right)\left(E_n^m + \frac{1}{2}\bar{c}i\omega F_n^m\right)\tilde{\theta} \tag{33}$$

where

$$E_n^m = \int_0^1 \phi_n^m \bar{r}^2\,\mathrm{d}\bar{r} = \int_0^1 \sqrt{1-\nu^2}\,\tilde{P}_n^m\,\mathrm{d}\nu \tag{34a}$$

$$F_n^m = \int_0^1 \phi_n^m \bar{r}\,\mathrm{d}\bar{r} = \int_0^1 \tilde{P}_n^m\,\mathrm{d}\nu \tag{34b}$$

$$B_{nj}^{mr} = \int_0^1 \phi_n^m \phi_j^r \bar{r}\,\mathrm{d}\bar{r} = \int_0^1 \tilde{P}_n^m \tilde{P}_j^r \frac{1}{\nu}\,\mathrm{d}\nu \tag{34c}$$

In Eq. (33), the superscript r can assume any integer between $-M$ $+M$, and m is summed from $-M$ to $+M$. However, the superscripts m and r on G, B, E, and F assume the absolute value of m and r.

The induced flow can then be expressed as

$$v(\bar{r},\hat{\psi},\bar{t}) = \sum_{n,m}\phi_n^m[\mathrm{Re}(\tilde{a}_n^m)\cos\omega\bar{t}\cos(m\hat{\psi}) - \mathrm{Im}(\tilde{a}_n^m)\sin\omega\bar{t}\cos(m\hat{\psi}) + \mathrm{Re}(\tilde{b}_n^m)\cos\omega\bar{t}\sin(m\hat{\psi}) - \mathrm{Im}(\tilde{b}_n^m)\sin\omega\bar{t}\sin(m\hat{\psi})] \tag{35}$$

For the reference blade, $\hat{\psi} = 0$; Eq. (35) becomes

$$v = \sum_{n,m}\phi_n^m[\mathrm{Re}(\tilde{a}_n^m)\cos\omega\bar{t} - \mathrm{Im}(\tilde{a}_n^m)\sin\omega t] \tag{36}$$

By substitution of Eq. (36) into Eq. (32), the resultant oscillatory lift can be expressed as

$$\begin{aligned}\text{lift} &= \bar{r}^2\tilde{\theta}\cos\omega\bar{t} - \frac{1}{2}\bar{r}\tilde{\theta}c\omega\sin(\omega\bar{t}) - \bar{r}\sum_{n,m}\phi_n^m[\mathrm{Re}(\tilde{a}_n^m)\cos\omega\bar{t} - \mathrm{Im}(\tilde{a}_n^m)\sin\omega t] \\ &= \left[\bar{r}^2\tilde{\theta} - \sum_{n,m}\phi_n^m\bar{r}\mathrm{Re}(\tilde{a}_n^m)\right]\cos\omega\bar{t} - \left[\frac{\tilde{\theta}}{2}\bar{c}\omega\bar{r} + \sum_{n,m}\phi_n^m\bar{r}\mathrm{Im}(\tilde{a}_n^m)\right]\sin\omega\bar{t} \\ &= \bar{r}^2\sqrt{\left(\tilde{\theta} - \sum_{n,m}\phi_n^m\mathrm{Re}(\tilde{a}_n^m)/\bar{r}\right)^2 + \left(\frac{\tilde{\theta}}{2}\bar{c}\omega/\bar{r} + \sum_{n,m}\phi_n^m\mathrm{Im}(\tilde{a}_n^m)/\bar{r}\right)^2} \\ &\times \cos\left(\omega\bar{t} + \tan^{-1}\left(\frac{\tilde{\theta}/2\ \bar{c}\omega/\bar{r} + \sum\phi_n^m\mathrm{Im}(\tilde{a}_n^m)/\bar{r}}{\tilde{\theta} - \sum\phi_n^m\mathrm{Re}(\tilde{a}_n^m)/\bar{r}}\right)\right)\end{aligned} \tag{37}$$

Thus, we have the magnitude and phase of lift due to $\tilde{\theta}$ corresponding to a lift deficiency function.

For a Q-bladed rotor, $\theta = \theta_0 + \tilde{\theta}\exp[i\omega(\bar{t} + \phi_q)]$, where the phasing of ϕ_q depends on the mode. For example, for a collective mode, $\phi_q = 0$, and for a two-bladed differential mode, $\phi_1 = 0$, $\phi_2 = \pi$. The impact of this phasing on Eq. (33) is simply to eliminate certain harmonics. For example, for a two-bladed collective mode, only even values of m and r remain. Thus, Eq. (37) and the lift deficiency function of m will depend on the number of blades and type of mode.

Results

Static Distribution

The three-dimensional, finite-state, unsteady wake model is now applied to the prediction of static and dynamic response of the induced flowfield. To begin, we consider the case of a one-bladed rotor with low lift in axial flow with $\theta = 1$. Thus, Eq. (33) can be simplified to be

$$\tilde{g}_j^r = \left[-imG_n^m\delta_{mr} + \left(2V\delta_{mr} + \frac{\sigma a}{4}\right)B_{nj}^{mr}\right]^{-1}\left(\frac{\sigma a}{4}\right)E_n^m \tag{38}$$

and the induced velocity distribution at the blade in the rotating system can be expressed by

$$v(\bar{r},\psi_1) = \sum_n[\mathrm{Re}(\tilde{a}_n^0)\phi_n^0 + 2\sum_{m=1}^{\infty}\mathrm{Re}(\tilde{a}_n^m)\phi_n^m] \tag{39}$$

Hence, the induced velocity at the blade is completely determined by the real part of the solution of $\tilde{g}_j^r$, and Eqs. (38) and (39) provide our steady solution for constant θ.

Figure 2a shows the resultant radial inflow distribution with $Q = 1$ and $S = 2$ (two shape functions per harmonic) for $M = 0$, 1, and 4, respectively. Parameters are $\sigma a = 0.2$ and $V = 0.05$. These data indicate that the computed inflow begins to climb near the tip as more harmonics are added. Figure 2b shows the effect as more radial functions are added with

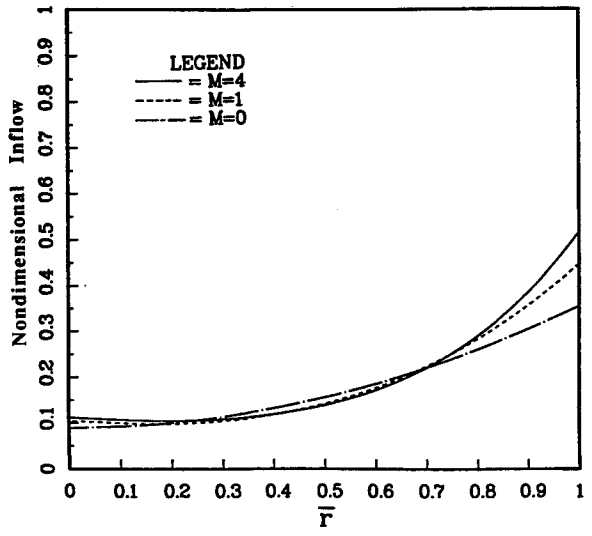

Fig. 2a Radial inflow distribution from Peters' model for various numbers of inflow harmonics with $S = 2$, $\sigma a = 0.2$, $V = 0.05$, and $\theta = 1$.

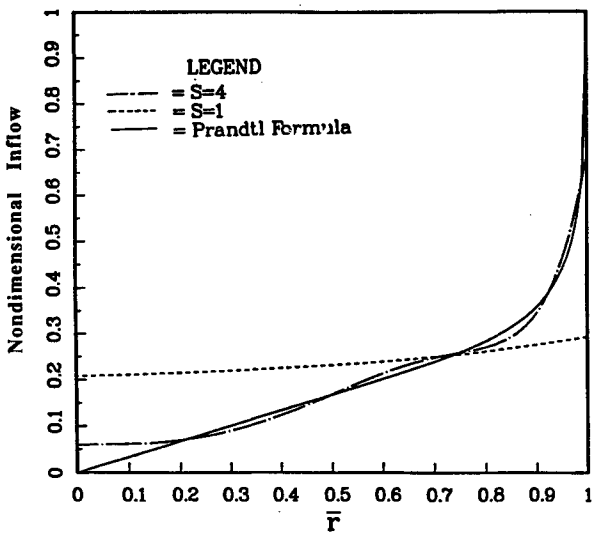

Fig. 2b Radial inflow distribution from Peters' model for various numbers of shape functions with $M = 4$, $\sigma a = 0.2$, $V = 0.05$, and $\theta = 1$.

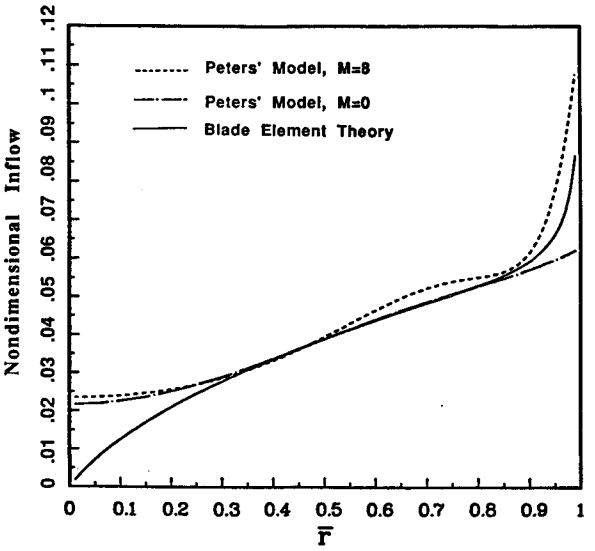

Fig. 3a Radial distribution of the inflow with $[B] \times [V]$, $\theta = 10$ deg, $\sigma a = 0.25$, and $S = 4$.

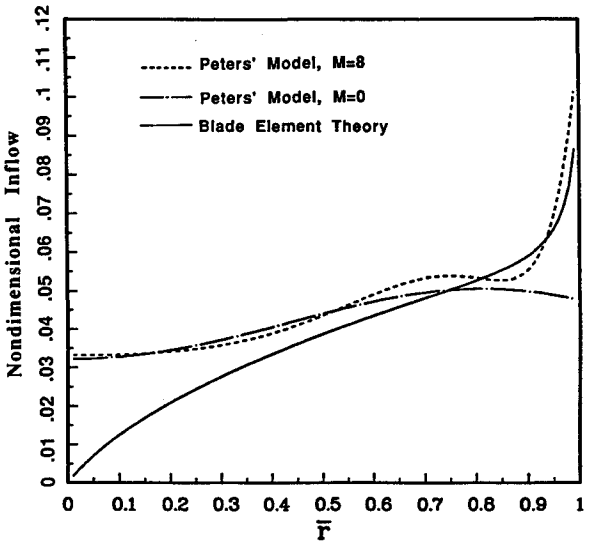

Fig. 3b Radial distribution of inflow with $[V] \times [B]$, $\theta = 10$ deg, $\sigma a = 0.25$, and $S = 4$.

$M = 4$. At $S = 4$, the solution (dash-dot line) has nearly converged to Prandtl's tip correction (solid line), which is essentially exact.

Next, we consider computation of induced flow in pure hover, which is a highly nonlinear condition. The computation of instantaneous induced inflow at the rotor disk consists of solving either of the systems Eqs. (17) or (18). Therefore, an iterative procedure is needed in order to determine the final V and the resultant inflow states. Normally, about five iterations are needed to converge.

Computations of the total inflow distribution with each version of the nonlinear model are presented in Figs. 3a and 3b, respectively. The collective pitch is 10 deg and $\sigma a = 0.25$. The computation is performed both for $M = 0$ and 8. The solid line is based on momentum theory with the tip loss correction function. Since the result with $M = 0$ is essentially the average induced flow, it quickly converges to momentum theory without any tip correction. The result with $M = 8$, on the other hand, is trying to match the tip loss solution ($v = 0.17$ at $\bar{r} = 1$). However, this convergence is slower. Another area of slow convergence is near the root. The polynomials ϕ_n^0 contain only even powers of $\bar{r}$. Thus, they converge slowly to the linear behavior near the blade root. Recall, however, that the intended use of our model is for aeroelasticity. Thus, these errors at the root and tip should not greatly affect generalized modal forces.

Further comparisions of Figs. 3a and 3b show that the result with $[B][V]$ is the more accurate, especially near the tip. Thus, Eq. (17) is used for the static flow in the data correlations to follow, and unsteady flow is taken as a perturbation about that iteratively determined static flow.

Unsteady

In this section, the resultant total induced flowfields both with and without unsteady pitch variations are compared with each other. Figures 4a–d represent the induced flow at a fixed point in space for $Q = 2$. ϕ_1 represents the angle between the azimuth of maximum blade pitch and the detection point. The time $\bar{t} = 0$ represents the time at which the blade passes the detection point. The collective pitch is 4 deg, maximum oscillatory pitch is 1 deg, and the oscillatory frequency is 4/rev. The phase shift due to the θ^* term in Eq. (27) is not included. The solid line is the case without the unsteady pitch variation $\tilde{\theta}$. Without the θ^* term, the largest positive (or negative) amount of average induced flow at the fixed point is

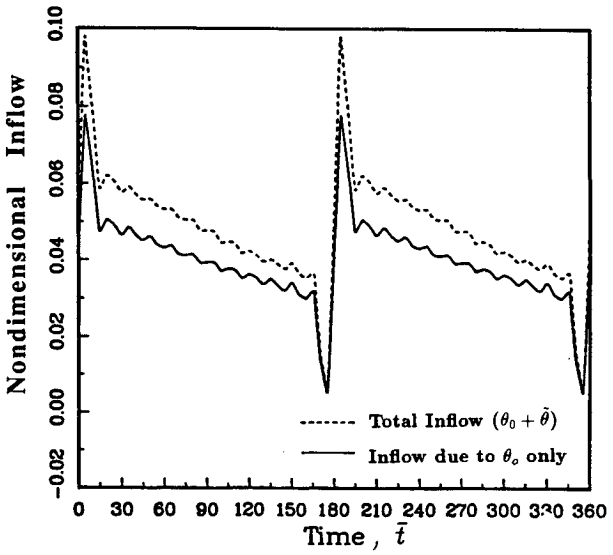

Fig. 4a Comparison of computed inflow with and without unsteady pitch at $\psi = 0$ deg vs spatial position of reference blade ($\psi_1 = \bar{t}$, deg): $Q = 2$; $\phi_2 = \phi_1 = 0$ deg; $M = 24$; $S = 3$; $\bar{r} = 0.824$; $\theta_q = 4$ deg + 1 deg cos4($\bar{t} + \phi_1$).

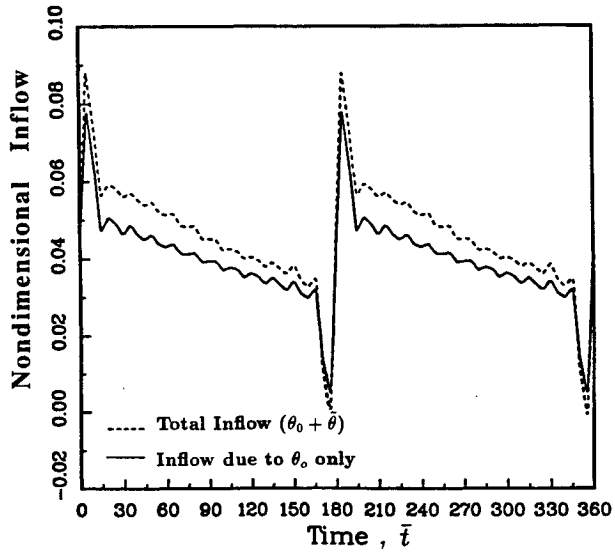

Fig. 4b Comparison of computed inflow with and without cyclic pitch at $\psi = 0$ deg vs spatial position of reference blade ($\psi_1 = \bar{t}$, deg): $Q = 2$; $\phi_1 = \phi_2 = 15$ deg; $M = 24$; $S = 3$; $\bar{r} = 0.824$.

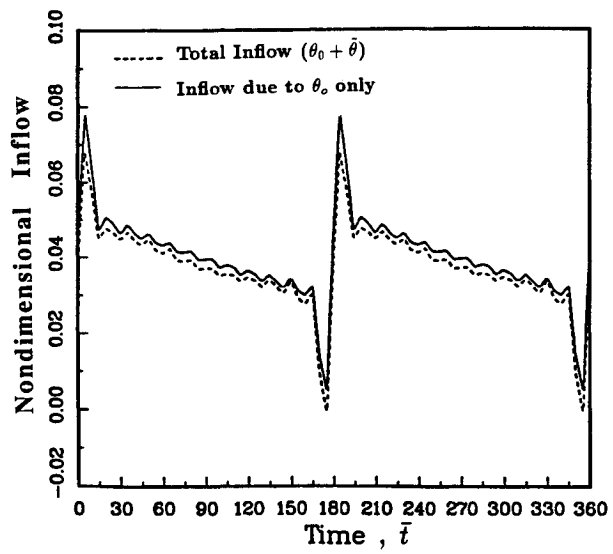

Fig. 4c Comparison of computed inflow with and without cyclic pitch at $\psi = 0$ deg vs spatial position of reference blade ($\psi_1 = \bar{t}$, deg): $Q = 2$; $\phi_1 = \phi_2 = 30$ deg; $M = 24$; $S = 3$; $\bar{r} = 0.824$.

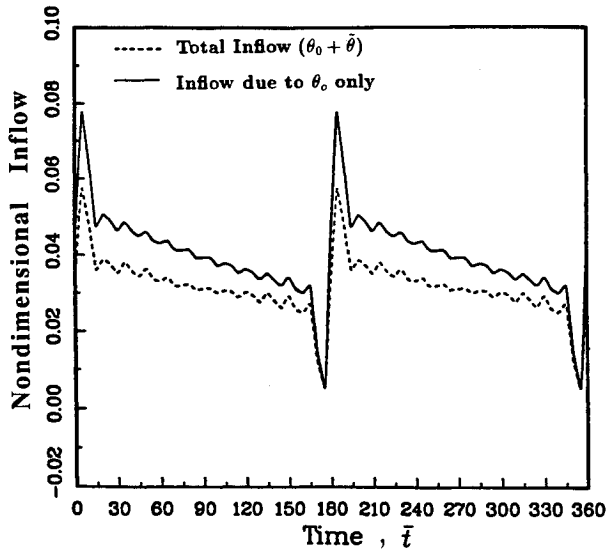

Fig. 4d Comparison of computed inflow with and without cyclic pitch at $\psi = 0$ deg vs spatial position of reference blade ($\psi_1 = \bar{t}$, deg): $Q = 2$; $\phi_1 = \phi_2 = 45$ deg; $M = 24$; $S = 3$; $\bar{r} = 0.824$.

found for the case in which the maximum (or minimum) pitch angle occurs precisely at the passage of the measurement point, $\phi_1 = 0$ or $\phi_1 = \pm 45$ deg. Figure 5 illustrates the behavior of the induced flowfield over the entire rotor disc at a particular instant in time. The time $\bar{t} = 0$ represents the time for which the blade is at its maximum pitch, 5 deg. A 4/rev pattern is clearly seen in the induced flow. This pattern is basically fixed in space as seen in the nonrotating system. Superimposed on this 4/rev pattern are the moving impulses caused by bound vorticity of the two blades.

Data Comparison

All of the experimental data used in this paper are from the laser Doppler velocimetry (LDV) measurements conducted in the AEROTECH.[16] A two-bladed Bell 212 teetering tail rotor is used. The rotor diameter is 2.59 m with a blade chord of 0.292 m. The induced velocity is measured at $z = 0.04$.

Comparisons of azimuthal variations in inflow velocity at $r/R = 0.765$ and 0.824 are shown in Figs. 6a and 6b. The collective pitch is still 4 deg, and unsteady pitch is zero. Good agreement can be seen everywhere on the flowfield with the exception of the doublet spike due to blade passage. These spikes are smaller in our model than in the data due to the truncation of our model at 24 harmonics. However, the inflow at the center of the doublet, which influences the angle of attack, is accurate. (If the angle of attack were in error, the inflow between blade passages would not agree.) When more harmonics are added, the computed spikes increase, but the lift stays constant.[6]

Finally, results with dynamic pitch for a collective mode are compared at $r/R = 0.765$, Fig. 6c. The steady pitch is 4 deg, and maximum dynamic excitation amplitude is 1 deg. The comparison is good, except (again) near the blade passage. It is also noted that this dynamic measurement is at a node in the unsteady inflow pattern. That is, it is at the boundary between upwash and downwash at which the unsteady induced flow is zero. This can be seen from the fact that the perturbation component is very small, as seen from the comparison in Fig. 7. For the computed results, the location of

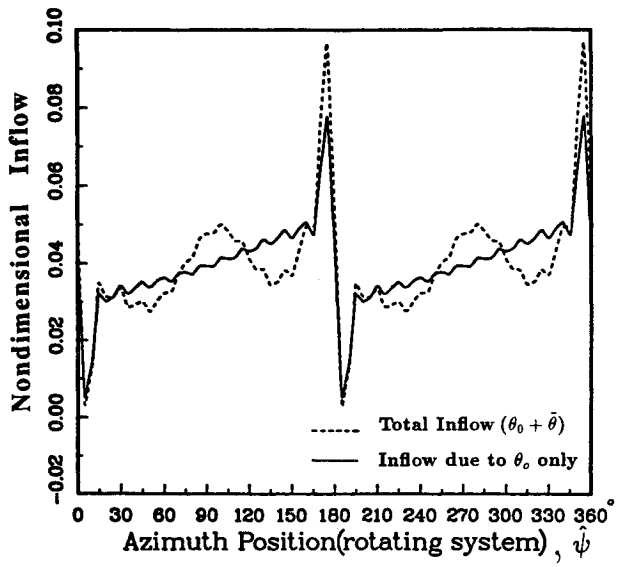

Fig. 5 Comparison of computed inflow with and without cyclic pitch: $Q = 2$, $\bar{t} = 0$; $M = 24$; $S = 3$; $\bar{r} = 0.824$.

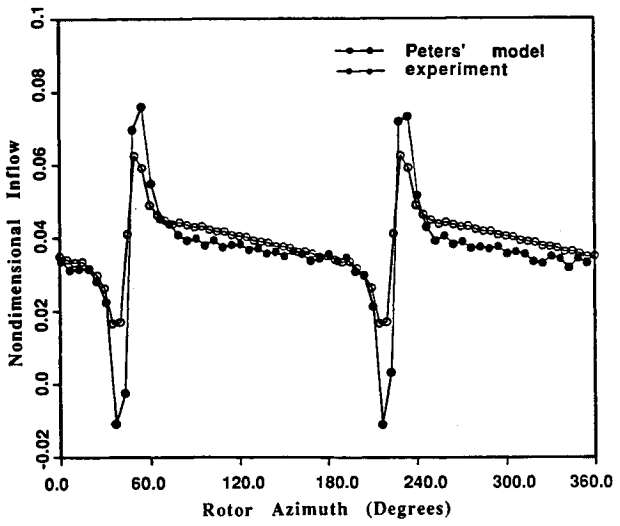

Fig. 6a Comparisons of calculated inflow with measured data at ψ = 45 deg vs spatial position of reference blade ($\psi_1 = \bar{t}$, deg): M = 24, $\bar{r} = 0.765$; $\sigma a = 0.9$; $\theta = 4$ deg.

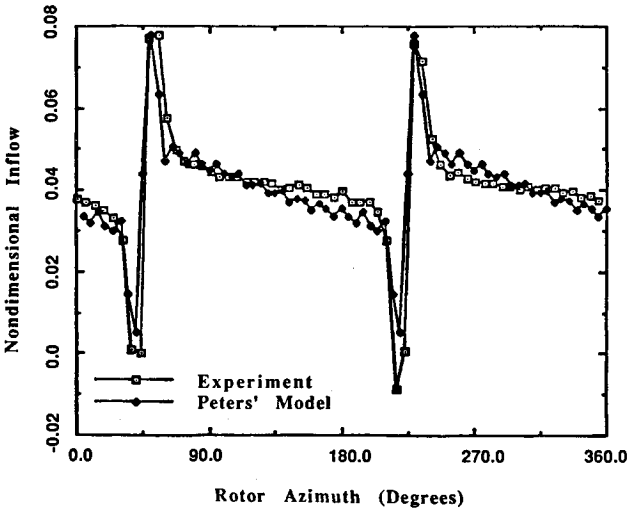

Fig. 6b Comparison of calculated inflow with measured data at ψ = 45 deg vs spatial position of reference blade ($\psi_1 = \bar{t}$, deg): M = 24; $\bar{r} = 0.824$; $\sigma a = 0.9$; $\theta = 4$ deg.

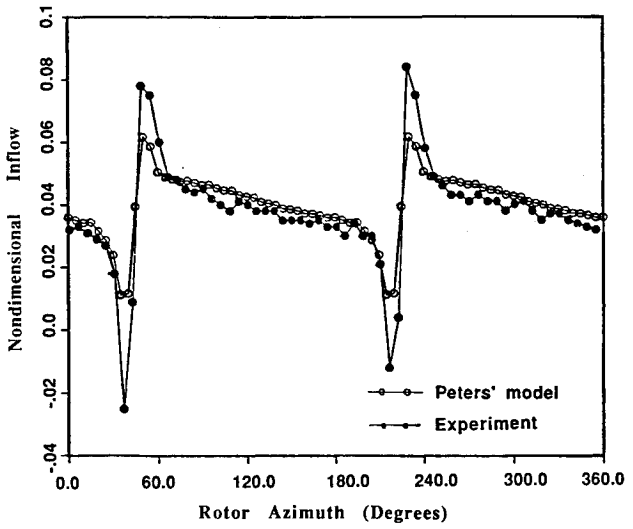

Fig. 6c Comparison of calculated inflow with measured data at ψ = 45 deg vs spatial position of reference blade ($\psi_1 = \bar{t}$, deg): M = 24; $\bar{r} = 0.765$; $\sigma a = 0.9$; $\theta = 4$ deg + 1 deg cos4($\bar{t}$ − 52 deg).

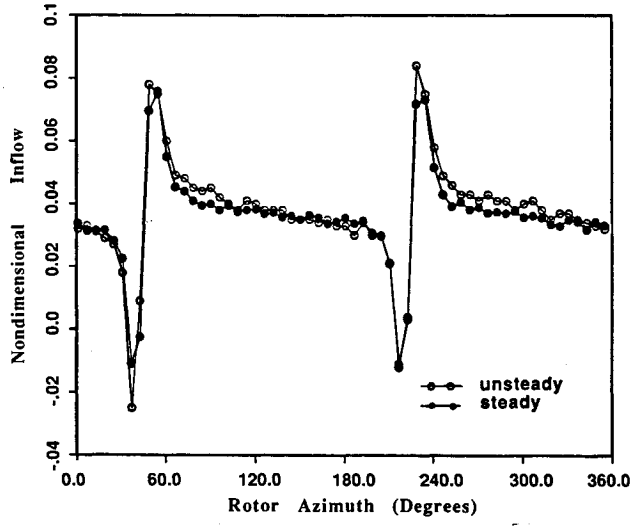

Fig. 7 Comparison of experimental steady and unsteady data from Figs 6a and 6c.

this node is significantly affected by the θ^* term in Eq. (27) (included in these calculations). Thus, the successful prediction of this node is a validation of the inflow model.

Comparison with Vortex-Lattice Method

We now turn to correlation with an unsteady, vortex-lattice, prescribed-wake model. This model is a thin lifting-surface theory, and the wake has been discretized into bound, shed, and trailing vortex filament fixed in a prescribed wake geometry.[3] The maximum oscillatory lift distribution is presented in Figs. 8a–d for both collective and differential modes for a two-bladed hovering rotor undergoing rigid pitch oscillations ($\bar{\theta} = 2$ deg cos $\omega\bar{t}$) about the steady condition θ_0 = 12 deg at $\omega = 3$/rev and 4/rev. The quasisteady theory has no induced-flow effects and is typical of present state-of-the-art rotor aeroelasticity work. The loss of lift due to inflow dynamics is significant in the differential mode at odd frequencies ($\omega = 3$) and in the collective mode at even frequencies ($\omega = 4$) since these modes are in resonance with the inflow. Also, the tip loss effect is clearly seen in those figures. The correlation between our model and the vortex-lattice model is excellent in most cases except at midspan for the differential mode at $\omega = 3$/rev. Our model shows higher loss

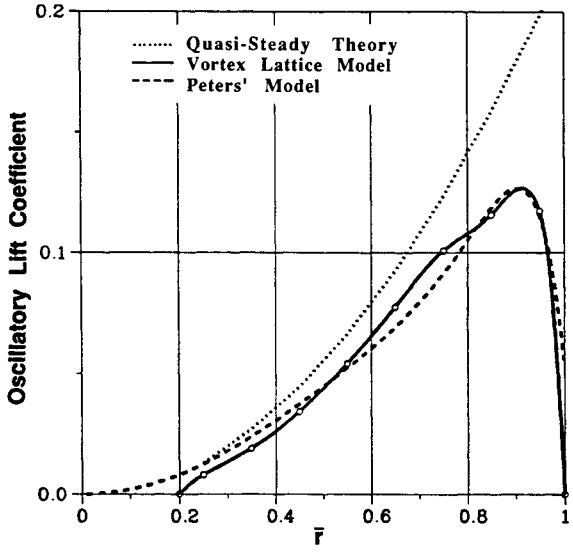

Fig. 8a Spanwise lift distribution, collective mode: $\omega = 3$; $Q = 2$; $\sigma a = 0.388$; $\theta_0 = 12$ deg; $\tilde{\theta} = 2$ deg; $M = 8$, $S = 3$.

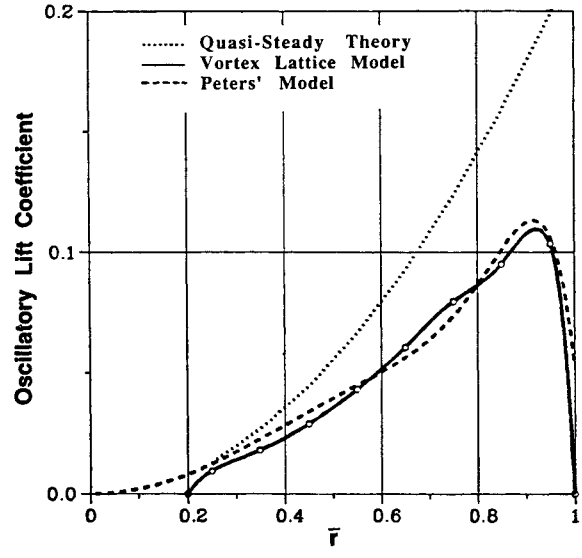

Fig. 8b Spanwise lift distribution, collective mode: $\omega = 4$; $Q = 2$; $\sigma a = 0.388$; $\theta_0 = 12$ deg; $\tilde{\theta} = 2$ deg; $M = 8$; $S = 3$.

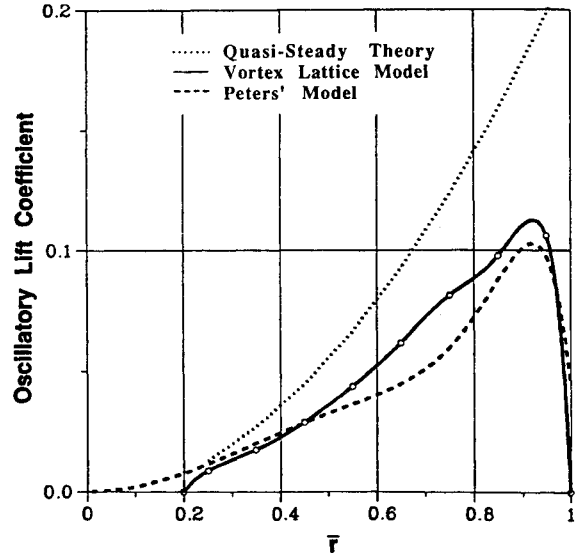

Fig. 8c Spanwise lift distribution, differential mode: $\omega = 3$; $Q = 2$; $\sigma a = 0.388$; $\theta_0 = 12$ deg; $\tilde{\theta} = 2$ deg; $M = 8$; $S = 3$.

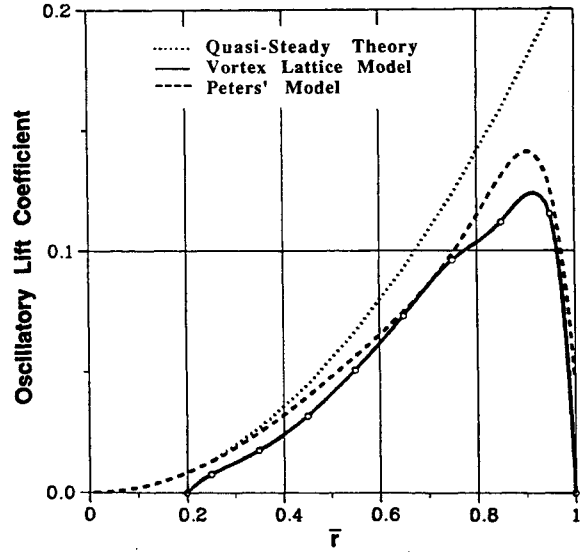

Fig. 8d Spanwise lift distribution, differential mode: $\omega = 4$; $Q = 2$; $\sigma a = 0.388$; $\theta_0 = 12$ deg; $\tilde{\theta} = 2$ deg; $M = 8$; $S = 3$.

of lift due to shed vorticity than does the vortex model at this frequency. Nearly identical comparisons result for $\omega = 1$/rev and 2/rev.

It should be mentioned that, in order to converge to the proper result, the vortex-lattice model must use 5-deg increments azimuthally and at least two wake layers beneath the rotor disk, which implies 576 elements of trailed and shed vortex filaments for each blade. In contrast, the finite-state model converges with eight harmonics and three shape functions. Therefore, the time-marching solution procedure of the vortex-lattice model requires about five times as much memory and computing time as does the finite-state solution, which involves only a single inversion of a matrix of order 51.

Conclusions

An unsteady, finite-state, three-dimensional induced-flow model has been successfully extended to included nonlinearities and then applied to the computation of the induced-flow distribution of a rotor in axial flow including hover. Numerical results have been compared against LDV measurements for both time-averaged and unsteady induced flow at the disk. In addition, the calculated oscillatory blade loadings are compared with those of a vortex-lattice method. The major conclusions of these comparisons are the following.

1) The time-averaged induced flow from the finite-state model gives good correlation with measured data at the radial positions shown.

2) The instantaneous induced-flow distribution is in excellent agreement with measured data. The blade-passage peaks are underpredicted by our model due to the truncation of harmonics, but the blade angle of attack and lift are well predicted.

3) Excellent overall correlation for unsteady airloads is obtained between the finite-state wake model and the more conventional vortex-lattice method. However, the finite-state model is more efficient.

4) The new wake model is ideally suited for aeroelastic analysis of rotors.

Acknowledgments

The theoretical developments in this paper were performed under funding from the Army Aeroflightdynamics Labora-

tory, NASA Grant NAG 2-462. The experimental measurements and data correlation were funded by the Army Research Office through the Georgia Institute of Technology Center of Excellence for Rotary Wing Aircraft Technology.

References

[1]Theodorsen, T., "General Theory of Aerodynamic Instabilities and the Mechanism of Flutter," NACA TR 496, 1949.

[2]Loewy, R. G., "A Two-Dimensional Approach to the Unsteady Aerodynamics of Rotary Wings," *Journal of Aerospace Sciences*, Vol. 24, No. 2, 1957, pp. 82–98.

[3]Yoo, K. M., "Unsteady Vortex Lattice Aerodynamics for Rotor Aeroelasticity in Hover and in Forward Flight," Ph.D. Dissertation, Georgia Inst. of Technology, School of Aerospace Engineering, Atlanta, GA, March 1990.

[4]Landgrebe, A. J., and Cheney, M. C., Jr., "Rotor Wakes—Keys to Performance Prediction," AGARD Specialists Meeting on The Aerodynamics of Rotary Wings, Marseille, France, AGARD-CP-111, Sept. 1972.

[5]Su, A., "Application of a State-Space Wake Model to Elastic Blade Flapping in Hover," Ph.D. Dissertation, Georgia Inst. of Technology, School of Aerospace Engineering, Atlanta, GA, Dec. 1989.

[6]He, C., "Development and Application of a Generalized Dynamic Wake Theory for Lifting Rotors," Ph.D. Dissertation, Georgia Inst. of Technology, School of Aerospace Engineering, Aug. 1989.

[7]Peters, D. A., Boyd, D. D., and He, C., "Finite-State Induced-Flow Model for Rotors in Hover and Forward Flight," *Journal of the American Helicopter Society*, Vol. 34, No. 4, Oct. 1989.

[8]Landgrebe, A. J., "An Analytical Method for Predicting Rotor Wake Geometry," *Journal of the American Helicopter Society*, Vol. 14, No. 4, Oct. 1969.

[9]Clark, D. R., and Leiper, A. C., "The Free Wake Analysis—A Method for the Prediction of Helicopter Rotor Hovering Performance," Proceedings of the 25th Annual National Forum of the American Helicopter Society, Washington, DC, May 1969; *Journal of the American Helicopter Society*, Vol. 15, No. 1, 1970.

[10]Kocurek, J. D., and Tangler, J. L., "A Prescribed Wake Lifting Surface Hover Performance Analysis," *Journal of the American Helicopter Society*, Vol. 22, No. 1, 1977, pp. 24–35.

[11]Peter, D. A., and He, C., "Comparison of Measured Induced Velocities with Results from a Closed-Form Finite-State Wake Model in Forward Flight," *Proceedings of the 45th Annual National Forum of the American Helicopter Society*, American Helicopter Society, Alexandria, VA, 1989, pp. 533–550.

[12]Peters, D. A., and Su, A., "The Effect of an Unsteady Three-Dimensional Wake on Elastic Blade-Flapping in Hover," *Proceedings of the 45th Annual Forum of the American Helicopter Society*, American Helicopter Society, Alexandria, VA, 1989, pp. 999–1015.

[13]Kinner, W., "Theory of Circular Wing," *Ingenieur Archiv*, Vol. 7, 1937, pp. 47, Translation No. 2345, Ministry of Aircraft Production, UK.

[14]Gaonkar, G. H., and Peter, D. A., "Review of Dynamic Inflow Modeling for Rotorcraft Flight Dynamics," *Proceedings of the AIAA SDM Conference*, AIAA, New York, 1986, pp. 89–115.

[15]Peters, D. A., and Ninh, H., "Dynamic Inflow for Practical Applications," *Journal of the American Helicopter Society*, Vol. 33, No. 4, Oct. 1988, pp. 64–68.

[16]Liou, S. G., and Komerath, N. M., "Inflow to a Rotor Blade Under Controlled Excitation," *Proceedings of the Fifteenth Southeastern Conference of Applied Mechanics*, Atlanta, GA, March 1990, pp. 711–717.